Proceedings of the 9th U.S. National and 10th Canadian Conference on Earthquake Engineering
Compte Rendu de la 9ième Conférence Nationale Américaine et
10ième Conférence Canadienne de Génie Parasismique
July 25-29, 2010, Toronto, Ontario, Canada • Paper No 589

CHARACTERISTICS OF EARTHQUAKE-INDUCED DIFFERENTIAL GROUND MOTIONS IN THE NEAR-FAULT REGION

G. P. Mavroeidis[1] and A. S. Papageorgiou[2]

ABSTRACT

In this study, time histories of the dynamic ground deformation field in the near-fault region are numerically computed using the approach proposed by Bouchon and Aki (1982). Four well-documented seismic events (i.e., 1979 Imperial Valley, 1985 Michoacan, 1989 Loma Prieta, and 1999 Izmit) are considered as case studies. The fault rupture is modeled as an aggregate of extended dislocation sources with rupture properties (e.g., slip, rise time, rupture velocity, etc) consistent with faulting models of the simulated earthquakes. The dynamic ground deformations are generated at selected locations coinciding with sites of accelerographs that recorded the ground excitation. The amplitude and waveform characteristics of strain, rocking, and torsional time histories in the near-fault region are discussed.

Introduction

Differential ground motions associated with seismic wave propagation induce dynamic ground deformations (i.e., strain, rocking, and torsion) that may have a significant impact on the dynamic response of extended engineering structures such as long-span bridges, dams, pipelines, tunnels, and high-rise buildings. Rosenblueth (1957) and Richter (1958) were the first researchers to point out that torsional ground motions may occur during an earthquake. A few years later, Newmark (1969) attributed the torsional effects to non-vertical incident seismic waves, approximated the twist of a foundation slab by the rotation of the free-field ground motion, and proposed a torsional spectrum to compute the displacements of a building due to torsional input. Since then, several researchers have investigated the effects of earthquake-induced strain, rocking, and torsional components of ground motion on engineering structures and proposed various methodologies to effectively incorporate them into engineering codes and design.

The recording of actual rotational ground motions excited by earthquakes is not a trivial task due to lack of technology for measuring small ground rotations precisely. Strong motion accelerographs provide the absolute ground motions at discrete locations during an earthquake; they do not reveal any direct information pertaining to differential motions. However, if the spacing between neighboring accelerograph sites is small (i.e., smaller than the wavelengths of

[1]Assistant Professor, Dept. of Civil Engineering, The Catholic University of America, Washington, DC 20064, USA
[2]Professor, Dept. of Civil Engineering, University of Patras, Patras 26500, Greece

the disturbances), indirect estimations of strain, rocking or torsion may be obtained. Therefore, the estimation of the dynamic ground deformation field may be achieved in places where a dense grid of strong motion instruments has been deployed. For instance, Niazi (1986) estimated the ground rocking during the 1979 Imperial Valley earthquake from the analysis of the three components of recorded accelerations along the El Centro linear differential array. Likewise, Oliveira and Bolt (1989) estimated the rotational components of seismic waves using data from the SMART-1 strong motion array in Taiwan. More recently, Gomberg (1997) developed an efficient method for estimating the complete time-varying dynamic ground deformation field from commonly available three-component single station seismic data and applied the methodology to study the correlation between dynamic ground deformation and structural damage using observations from the 1994 Northridge earthquake.

In the absence of near-fault records of differential ground motions, the synthesis of strain, rocking, and torsional input (adequate for earthquake engineering applications) becomes an important issue. In general, there are two approaches to the subject. The first approach is based on the derivation of a response spectrum for the rotational components of seismic ground motion from a harmonic translational component at the surface (Trifunac, 1982) and the development of torsional and rocking accelerograms compatible with an artificial translational accelerogram that includes surface and body waves at a given proportion (Lee and Trifunac, 1985, 1987). The second approach exploits physical models of the source and wave propagation processes for the numerical simulation of strain, rocking, and torsional time histories. Bouchon and Aki (1982) (see also Bouchon et al., 1982) simulated time histories of the dynamic ground deformation field (i.e., strain, rocking, and torsion) in the vicinity of earthquake faults embedded in a layered halfspace using the discrete wavenumber representation method (Bouchon and Aki, 1977; Bouchon, 1979).

In this study, time histories of the dynamic ground deformation field in the near-fault region are numerically computed using the approach proposed by Bouchon and Aki (1982). Four well-documented seismic events (i.e., 1979 Imperial Valley, 1985 Michoacan, 1989 Loma Prieta, and 1999 Izmit) are considered as case studies.

Theory Elements

The linearized theory of elasticity is frequently used in seismology (see e.g., Aki and Richards, 1980; Dahlen and Tromp, 1998). Under the assumption of continuous, smooth, and small displacements, the deformation tensor (E_{ij}) at a point with Cartesian coordinates (x, y, z) may be defined (see e.g., Malvern, 1969) in terms of the partial derivatives of the components of the displacement vector, $\boldsymbol{u} = (u_x, u_y, u_z)^T$, as:

$$E_{ij} = \begin{bmatrix} \frac{\partial u_x}{\partial x} & \frac{\partial u_x}{\partial y} & \frac{\partial u_x}{\partial z} \\ \frac{\partial u_y}{\partial x} & \frac{\partial u_y}{\partial y} & \frac{\partial u_y}{\partial z} \\ \frac{\partial u_z}{\partial x} & \frac{\partial u_z}{\partial y} & \frac{\partial u_z}{\partial z} \end{bmatrix} \tag{1}$$

The multiplication of the deformation tensor (E_{ij}) by $\boldsymbol{dr} = (dx, dy, dz)^T$ yields the deformation (or relative displacement) vector, $\boldsymbol{du} = (du_x, du_y, du_z)^T$, of the differential element dx, dy, dz.

The deformation tensor (E_{ij}) can be resolved into a symmetric strain tensor (ε_{ij}) and an asymmetric rotational tensor (ω_{ij}):

$$E_{ij} = \varepsilon_{ij} + \omega_{ij} \tag{2}$$

where

$$\varepsilon_{ij} = \begin{bmatrix} \dfrac{\partial u_x}{\partial x} & \dfrac{1}{2}\left(\dfrac{\partial u_x}{\partial y} + \dfrac{\partial u_y}{\partial x}\right) & \dfrac{1}{2}\left(\dfrac{\partial u_x}{\partial z} + \dfrac{\partial u_z}{\partial x}\right) \\ \dfrac{1}{2}\left(\dfrac{\partial u_y}{\partial x} + \dfrac{\partial u_x}{\partial y}\right) & \dfrac{\partial u_y}{\partial y} & \dfrac{1}{2}\left(\dfrac{\partial u_y}{\partial z} + \dfrac{\partial u_z}{\partial y}\right) \\ \dfrac{1}{2}\left(\dfrac{\partial u_z}{\partial x} + \dfrac{\partial u_x}{\partial z}\right) & \dfrac{1}{2}\left(\dfrac{\partial u_z}{\partial y} + \dfrac{\partial u_y}{\partial z}\right) & \dfrac{\partial u_z}{\partial z} \end{bmatrix} = \begin{bmatrix} \varepsilon_{xx} & \dfrac{\gamma_{xy}}{2} & \dfrac{\gamma_{xz}}{2} \\ \dfrac{\gamma_{xy}}{2} & \varepsilon_{yy} & \dfrac{\gamma_{yz}}{2} \\ \dfrac{\gamma_{xz}}{2} & \dfrac{\gamma_{yz}}{2} & \varepsilon_{zz} \end{bmatrix} \tag{3}$$

and

$$\omega_{ij} = \begin{bmatrix} 0 & \dfrac{1}{2}\left(\dfrac{\partial u_x}{\partial y} - \dfrac{\partial u_y}{\partial x}\right) & \dfrac{1}{2}\left(\dfrac{\partial u_x}{\partial z} - \dfrac{\partial u_z}{\partial x}\right) \\ \dfrac{1}{2}\left(\dfrac{\partial u_y}{\partial x} - \dfrac{\partial u_x}{\partial y}\right) & 0 & \dfrac{1}{2}\left(\dfrac{\partial u_y}{\partial z} - \dfrac{\partial u_z}{\partial y}\right) \\ \dfrac{1}{2}\left(\dfrac{\partial u_z}{\partial x} - \dfrac{\partial u_x}{\partial z}\right) & \dfrac{1}{2}\left(\dfrac{\partial u_z}{\partial y} - \dfrac{\partial u_y}{\partial z}\right) & 0 \end{bmatrix} = \begin{bmatrix} 0 & -\omega_z & \omega_y \\ \omega_z & 0 & -\omega_x \\ -\omega_y & \omega_x & 0 \end{bmatrix} \tag{4}$$

The diagonal elements of the strain tensor (ε_{ij}) provide the axial strains of the orthogonal differential baselengths, while the off-diagonal elements provide the shear strains (or half the angle changes) between orthogonal differential baselengths. On the other hand, the off-diagonal components of the rotational tensor (ω_{ij}) provide the rotations of the differential element around the x, y, and z axes. If two of the axes lie on the horizontal plane and the third axis is along the vertical direction, then the terms "rocking" and "torsion" may alternatively be utilized to describe the rotations along the horizontal and vertical axes, respectively.

With the assumption that the x and y axes are parallel and transverse, respectively, to the fault strike, while z is along the vertical direction, the stress-free boundary conditions at the free surface imply that the shear strains ε_{xz} and ε_{yz} are zero; that is:

$$\frac{1}{2}\left(\frac{\partial u_x}{\partial z} + \frac{\partial u_z}{\partial x}\right) = 0 \quad \Rightarrow \quad \frac{\partial u_x}{\partial z} = -\frac{\partial u_z}{\partial x} \tag{5a}$$

$$\frac{1}{2}\left(\frac{\partial u_y}{\partial z} + \frac{\partial u_z}{\partial y}\right) = 0 \quad \Rightarrow \quad \frac{\partial u_y}{\partial z} = -\frac{\partial u_z}{\partial y} \tag{5b}$$

Using Eq. 5, the rocking ground motion components of Eq. 4 may then be written as:

$$\omega_x = \frac{\partial u_z}{\partial y}, \quad \omega_y = -\frac{\partial u_z}{\partial x} \tag{6}$$

Computational Method

Bouchon and Aki (1982) simulated time histories of the dynamic ground deformation field (i.e., strain, rocking, and torsion) in the vicinity of strike-slip and dip-slip faults embedded in a layered halfspace using the discrete wavenumber representation method (Bouchon and Aki, 1977; Bouchon, 1979). The basic idea of this methodology is the representation of the elastic wave field by a superposition of plane waves propagating in discrete directions. According to the Helmholtz's decomposition theorem for vector fields, the displacement vector, $\boldsymbol{u} = (u_x, u_y, u_z)^T$, may be resolved into the gradient of a scalar displacement potential and the curl of a vector displacement potential (with the displacement potentials being the solutions of the wave equations). By representing the seismic dislocations by their body-force equivalents (Burridge and Knopoff, 1964) and following the procedure proposed by Bouchon (1979), the discrete representation of the displacement potentials (and thus of the displacement and stress vectors) in the wavenumber domain is obtained. Subsequently, the discrete wavenumber representation of the deformation tensor (E_{ij}) can be derived by differentiating the components of the displacement vector. As a result, closed-form expressions for the elements of the deformation tensor are obtained in terms of the displacement potentials (or, equivalently, in terms of the components of the displacement and stress vectors).

Simulation Results

Four well-documented seismic events are considered in this study; namely, the 1979 Imperial Valley, the 1985 Michoacan, the 1989 Loma Prieta, and the 1999 Izmit earthquakes (see Mavroeidis and Papageorgiou, 2010). The selected seismic events cover a wide range of moment magnitudes (i.e., M_w 6.5-8.1), fault mechanisms (i.e., strike slip, reverse, oblique), and tectonic environments (i.e., interplate, subduction). Fig. 1 provides map views of the epicentral regions of all four earthquakes including the projection of the idealized fault planes on the free surface and the location of strong motion instruments that recorded the ground shaking. Several researchers have extensively studied the fault rupture process of the aforementioned seismic events, and inferred the spatial and temporal slip distribution on the causative fault planes. Table 1 summarizes basic parameters pertaining to the source mechanism of the selected earthquakes with reference to the preferred faulting models; these idealized models of the earthquake source will be used for the computation of the components of the deformation tensor (E_{ij}) of Eq. 1 on selected locations in the immediate vicinity of the tectonic fault. Once the elements of E_{ij} are known, the strain, rocking, and torsional components can be calculated by using Eq. 3 and 4.

Table 1. Earthquakes and faulting models considered in the present study.

Location	M_w	Date	Mechanism	Slip Model Reference	Source Modeling Data
Imperial Valley, USA	6.5	15-Oct-79	Strike Slip	Archuleta (1984)	Strong Motion
Michoacan, Mexico	8.1	19-Sep-85	Reverse	Mendoza and Hartzell (1989)	Strong Motion, Teleseismic
Loma Prieta, USA	6.9	17-Oct-89	Oblique	Zeng et al. (1993)	Strong Motion
Izmit, Turkey	7.5	17-Aug-99	Strike Slip	Bouchon et al. (2002)	Strong Motion

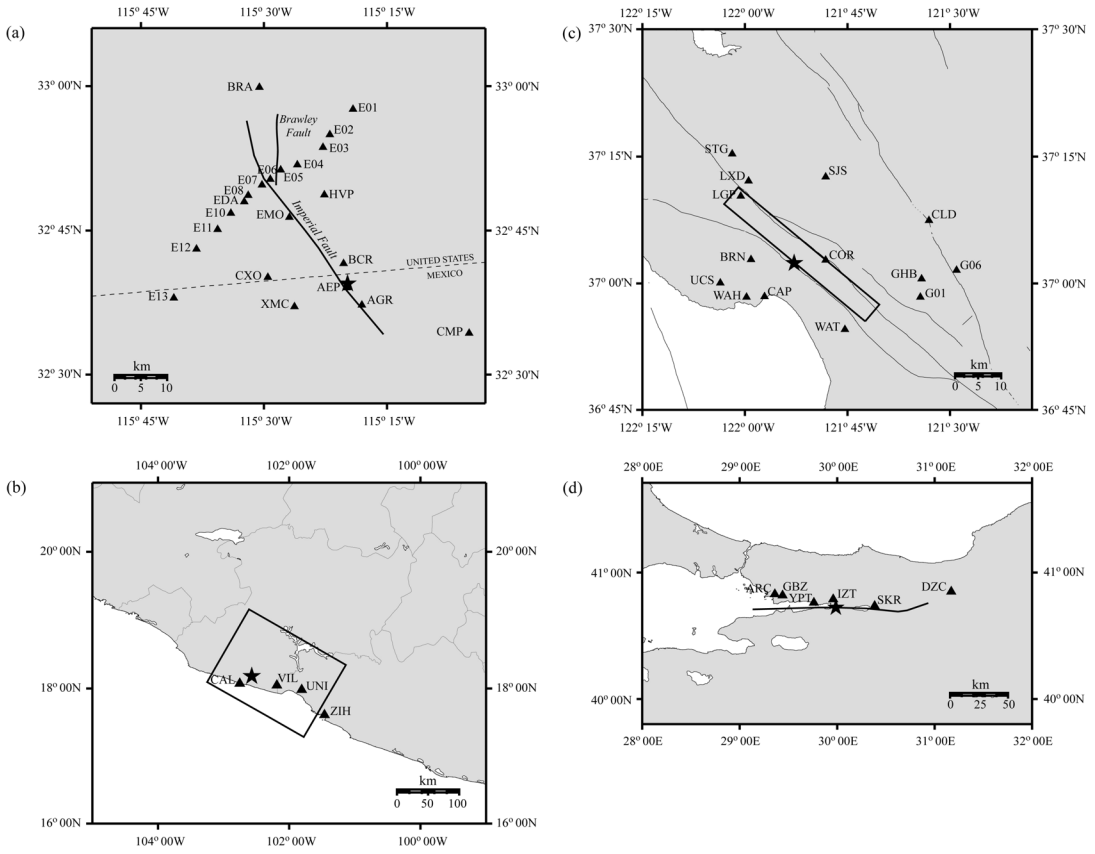

Figure 1. Map views of (a) the 1979 Imperial Valley, (b) the 1985 Michoacan, (c) the 1989 Loma Prieta, and (d) the 1999 Izmit earthquakes.

Discussion

Figures 2-5 display the synthetic time series of all components of the deformation tensor (E_{ij}) for selected stations of Fig. 1. The following observations can be made:

- The axial strains are characterized by relatively small amplitudes with the exception of strains in the transverse direction (i.e., $\partial u_y/\partial y$) for specific stations in the immediate vicinity of the 1979 Imperial Valley fault (i.e., stations E06, E07 and E08 in Figure 2). Furthermore, the results illustrate that extension in one horizontal direction is associated with compression in the other horizontal direction.
- The amplitudes of the torsional components of the dynamic ground deformation field are typically larger than the amplitudes of the respective rocking components. Furthermore, while rocking along the strike-parallel direction is larger than rocking along the strike-normal direction for the 1979 Imperial Valley earthquake, there is no clear trend for the other three earthquakes considered in the present study.
- Torsion and rocking components of ground motion obtained along a transverse profile to the fault trace reveal that peak rotations decrease quite rapidly with distance to the fault. This observation becomes more apparent if results of additional receiver points, not shown here, are also considered.

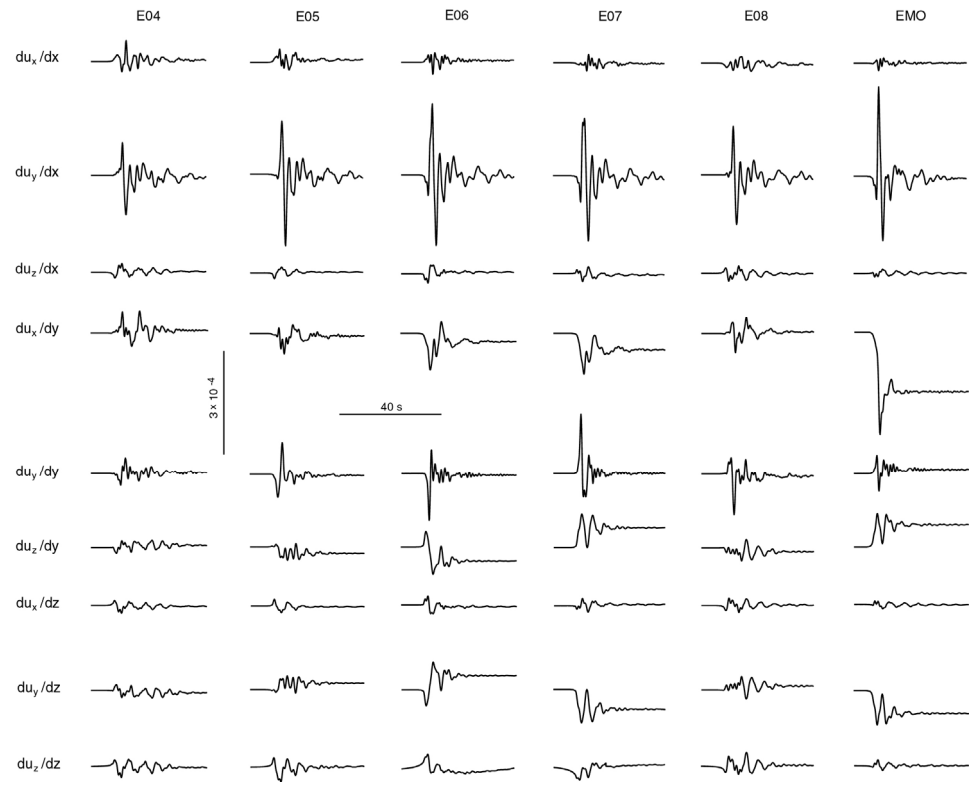

Figure 2. Time series of the deformation tensor components (E_{ij}) for selected stations of the 1979 Imperial Valley earthquake.

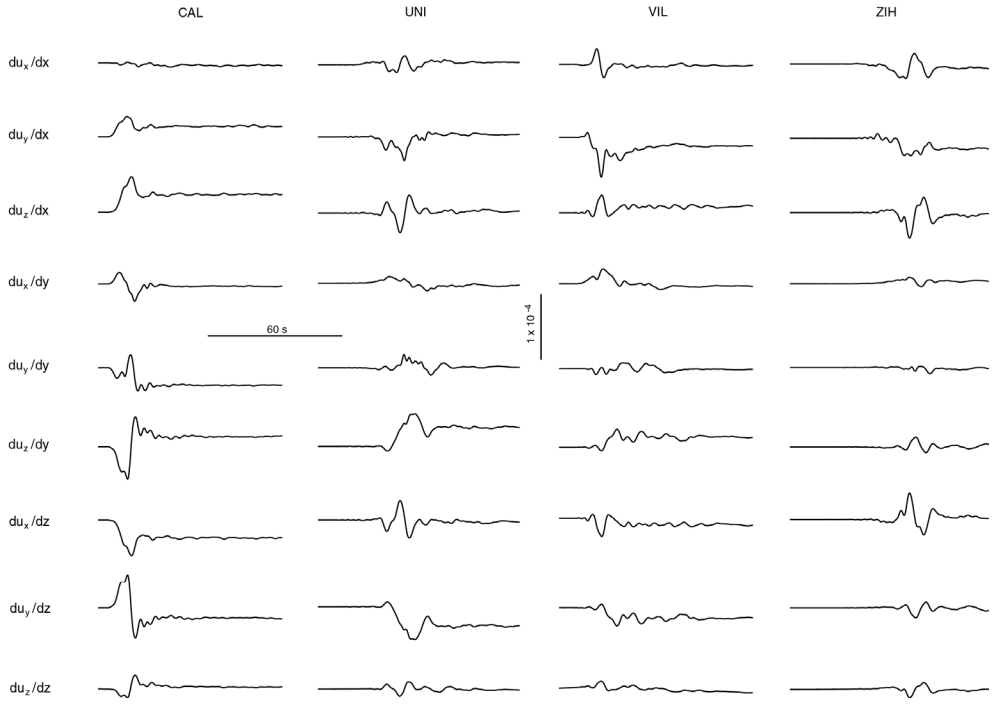

Figure 3. Time series of the deformation tensor components (E_{ij}) for selected stations of the 1985 Michoacan earthquake.

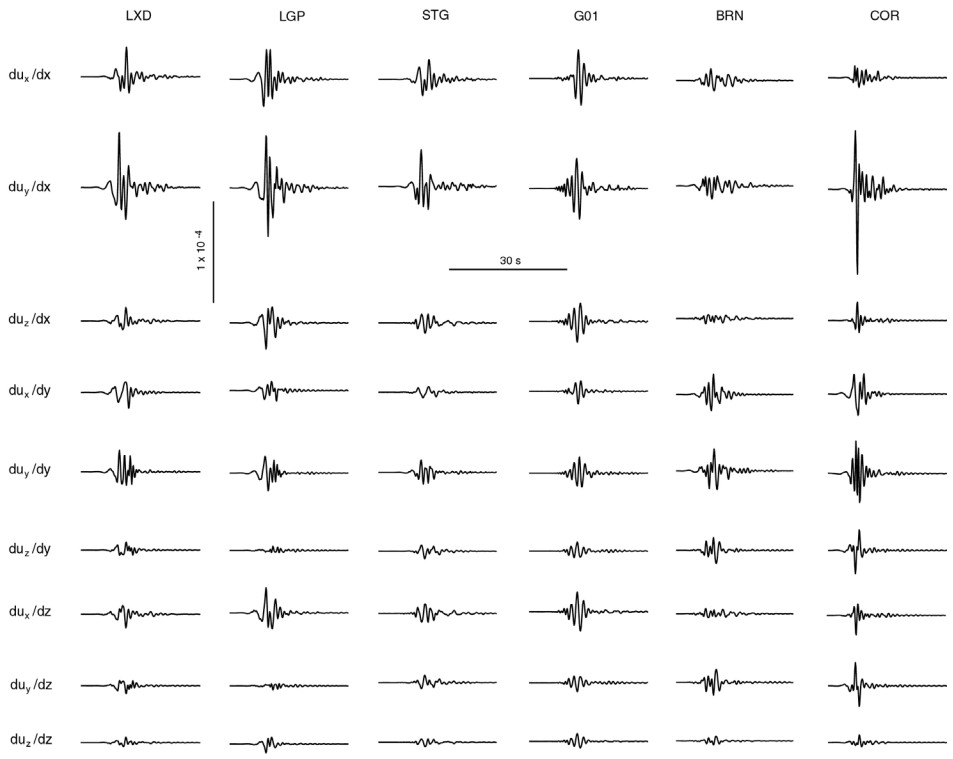

Figure 4. Time series of the deformation tensor components (E_{ij}) for selected stations of the 1989 Loma Prieta earthquake.

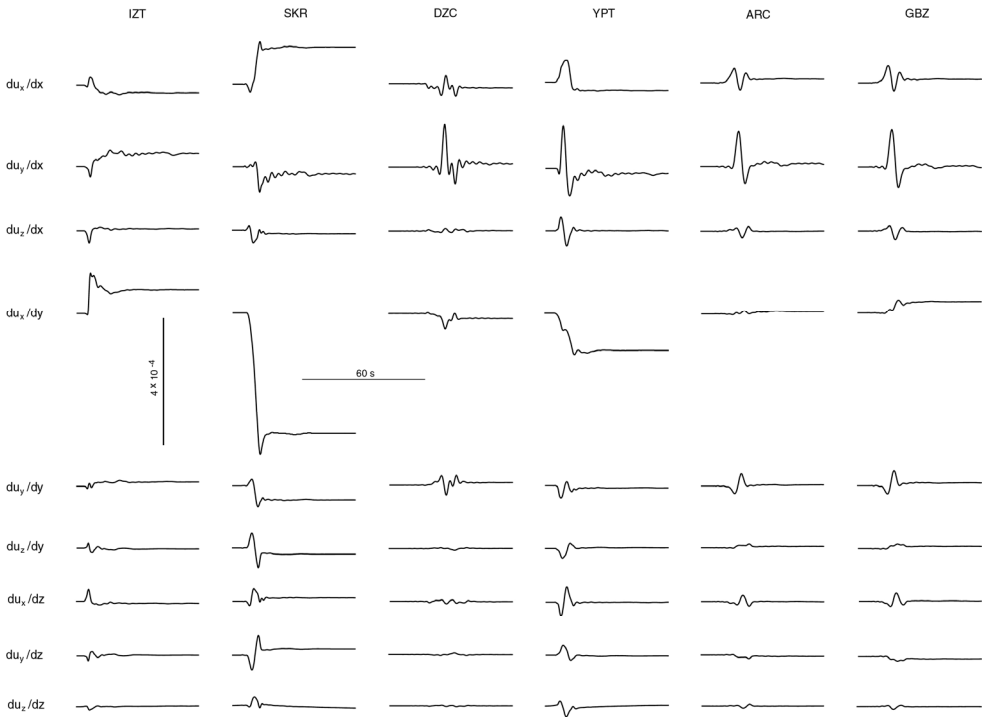

Figure 5. Time series of the deformation tensor components (E_{ij}) for selected stations of the 1999 Izmit earthquake.

- Stations E07 and EMO are located at approximately the same distance from the fault trace (see Figure 1). The time series of the deformation tensor components (E_{ij}) for these two stations exhibit comparable amplitude and waveform characteristics with the exception of the peak values of $\partial u_x/\partial y$ that affect both the shear strain between the x and y directions (i.e., $\gamma_{xy}/2$) and the torsional component (i.e., ω_z). The peak value of $\partial u_x/\partial y$ at EMO is roughly three times larger than the peak value of $\partial u_x/\partial y$ at E07. The difference in amplitude may be attributed to the large amount of slip (and perhaps to the supershear rupture velocity) over the part of the fault adjacent to EMO station. This observation indicates that variations of slip (and rupture velocity) over the fault plane may affect the variation of differential ground motions.
- The simulation results indicate that the peak values of rocking and torsion at the stations depicted in Figs. 2 and 5 were of the order of 10^{-4} rad and 2.5 10^{-4} rad, respectively. These values are in good agreement with estimates of ground rotations available in the literature based on actual strong motion data. For instance, the peak rotation amplitudes estimated by Niazi (1986) from analysis of the three components of recorded accelerations along the El Centro linear differential array during the 1979 Imperial Valley earthquake were in the range of 10^{-4} to 3 10^{-4} rad (when larger station distances were considered in the analysis).

The top three panels of Fig. 6 display the time series of the $\partial u_x/\partial x$, $\partial u_y/\partial x$, and $\partial u_z/\partial x$ components of the deformation tensor (E_{ij}) for selected stations of the 1979 Imperial Valley earthquake. The bottom three panels illustrate the three components of the velocity time histories generated at the same locations. Comparison of these two sets of data reveals a remarkable similarity (at least over the segment of intense ground motion) between the waveforms of the velocity time histories and the derivatives of the displacement components with respect to distance along the fault strike (i.e., x coordinate). As pointed out by Bouchon and Aki (1982), this indicates that most of the energy (which controls the peak amplitudes of motion) propagates at each observation point within a relatively small range of phase velocities and thus the relationship

$$\frac{\partial u_i}{\partial x} \approx -\frac{1}{c}\frac{\partial u_i}{\partial t} \tag{7}$$

(with c being the average phase velocity) is approximately valid.

The phase velocities may be estimated from the synthetic time histories of Fig. 6 using Eq. 7. For the depicted stations, the estimated phase velocities turn out to be close to the shear wave velocity of the basement rock (4 to 5 km/s). This observation confirms the proposition that phase velocities are controlled either by the basement rock shear velocity or the rupture velocity, and not by the shear wave velocity of unconsolidated sediments (e.g., Luco and Sotiropoulos, 1980; Bouchon and Aki, 1982). Since the rupture velocity of the 1979 Imperial Valley earthquake was highly variable, the relationship between phase and rupture velocities for this particular seismic event is rather unclear. As pointed out by Trifunac and Lee (1997), the determination of a site-specific phase velocity is still debatable and is likely to remain so until more field data become available.

Therefore, the axial strain along the strike direction ($\varepsilon_{xx} = \partial u_x/\partial x$), the rocking along the transverse direction ($\omega_y = -\partial u_z/\partial x$), and the torsional motion ($\omega_z \approx 0.5*\partial u_y/\partial x$, *assuming* that the dynamic displacement is primarily transverse to the fault in a relatively narrow zone along the

fault strike; see e.g., Bouchon et al., 1982) may be estimated with reasonable accuracy through Eq. 7 by using synthetic (or actual) ground velocities and properly selected phase velocities. We would like to point out that the analytical model proposed by Mavroeidis and Papageorgiou (2003) for the representation of long-period (coherent) component of the near-fault ground motion (along with properly selected phase velocities) may be exploited to approximate the torsional component of the near-fault ground motion.

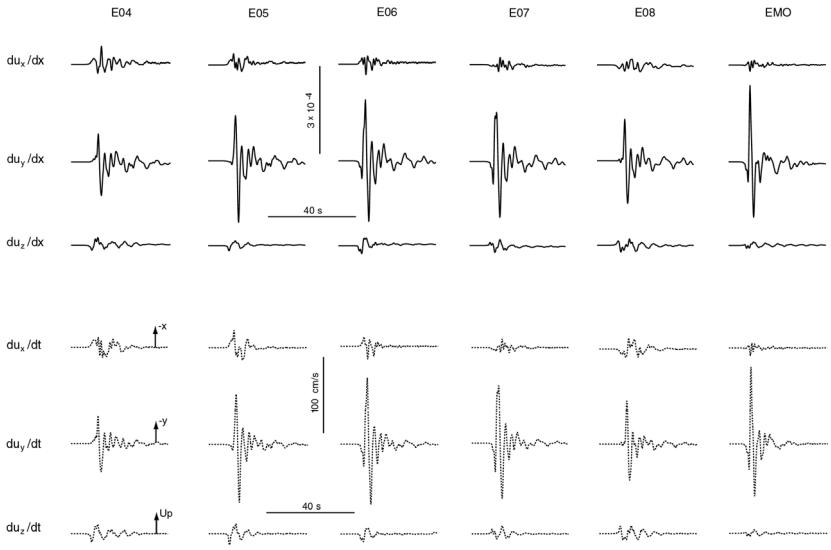

Figure 6. Comparison between time series of specific components of the deformation tensor (i.e., $\partial u_i/\partial x$, $i=x, y, z$) and time histories of the ground velocity components (i.e., $\partial u_i/\partial t$, $i=x, y, z$) for selected stations of the 1979 Imperial Valley earthquake.

Summary

The primary characteristics of strain, rocking, and torsional components of ground motion in the near-fault region induced by seismic excitations were discussed using the approach proposed by Bouchon and Aki (1982). The 1979 Imperial Valley, 1985 Michoacan, 1989 Loma Prieta, and 1999 Izmit earthquakes were considered as cases studies. The simulation results were obtained assuming a flat layer crustal model. While this approximation is adequate for several cases, it may not be accurate for cases characterized by significant lateral heterogeneities (e.g., sedimentary basins, irregular topography, etc; see e.g., Papageorgiou, 1992).

Acknowledgments

This research was partially supported by the U.S. Geological Survey (USGS), Department of the Interior, under USGS Award Number 04HQGR0029. The authors would like to thank Drs. Ralph Archuleta, Michel Bouchon, Carlos Mendoza, and Yuehua Zeng for providing the fault slip models used in this study.

References

Aki, K., and P. G. Richards (1980). *Quantitative Seismology: Theory and Methods*, W. H. Freeman, New York, NY.

Archuleta, R. J. (1984). A faulting model for the 1979 Imperial Valley earthquake, *J. Geophys. Res.* 89, 4559-4585.

Bouchon, M. (1979). Discrete wave-number representation of elastic wave fields in three-space

dimensions, *J. Geophys. Res.* 84, 3609-3614.
Bouchon, M., and K. Aki (1977). Discrete wave-number representation of seismic-source wave fields, *Bull. Seism. Soc. Am.* 67, 259-277.
Bouchon, M., and K. Aki (1982). Strain, tilt, and rotation associated with strong ground motion in the vicinity of earthquake faults, *Bull. Seism. Soc. Am.* 72, 1717-1738.
Bouchon, M., K. Aki, and P.-Y. Bard (1982). Theoretical evaluation of differential ground motions produced by earthquakes, in *Proc. of the Third International Earthquake Microzonation Conference*, Seattle, WA, June 28-July 1, 1982.
Bouchon, M., M. N. Töksoz, H. Karabulut, M.-P. Bouin, M. Dietrich, M. Aktar, and M. Edie (2002). Space and time evolution of rupture and faulting during the 1999 Izmit (Turkey) earthquake, *Bull. Seism. Soc. Am.* 92, 256-266.
Burridge, R., and L. Knopoff (1964). Body force equivalents for seismic locations, *Bull. Seism. Soc. Am.* 54, 1875-1888.
Dahlen, F. A., and J. Tromp (1998). *Theoretical Global Seismology*, Princeton University Press, Princeton, NJ.
Gomberg, J. (1997). Dynamic deformations and the M 6.7 Northridge, California, earthquake, *Soil Dyn. Earthquake Engng.* 16, 471-494.
Lee, V. M., and M. D. Trifunac (1985). Torsional accelerograms, *Soil Dyn. Earthquake Engng.* 4, 132-139.
Lee, V. W., and M. D. Trifunac (1987). Rocking strong earthquake accelerations, *Soil Dyn. Earthquake Engng.* 6, 75–89.
Luco, J. E., and D. A. Sotiropoulos (1980). Local characterization of free-field ground motion and effects of wave passage, *Bull. Seism. Soc. Am.* 70, 2229-2244.
Malvern, L. E. (1969). *Introduction to the Mechanics of a Continuous Medium*, Prentice-Hall, Upper Saddle River, NJ.
Mavroeidis, G. P., and A. S. Papageorgiou (2003). A mathematical representation of near-fault ground motions, *Bull. Seism. Soc. Am.* 93, 1099-1131.
Mavroeidis, G. P., and A. S. Papageorgiou (2010). Effect of fault rupture characteristics on near-fault ground motions, *Bull. Seism. Soc. Am.* 100, 37-58.
Mendoza, C., and S. H. Hartzell (1989), Slip distribution of the 19 September 1985 Michoacan, Mexico, earthquake: Near-source and teleseismic constraints, *Bull. Seism. Soc. Am.* 79, 655-669.
Newmark, N. M. (1969). Torsion in symmetrical buildings, in *Proc. of the Fourth World Conference on Earthquake Engineering (4WCEE)*, Santiago, Chile.
Niazi, M. (1986). Inferred displacements, velocities and rotations of a long rigid foundation located at El Centro differential array site during the 1979 Imperial Valley, California, earthquake, *Earthquake Engrg. Struct. Dyn.* 14, 531-542.
Oliveira, C. S., and B. A. Bolt (1989). Rotational components of surface strong ground motion, *Earthquake Engrg. Struct. Dyn.* 18, 517-526.
Papageorgiou, A. S. (1992). Differential motions in sedimentary valleys, in *Proc. of the ASCE Specialty Conference on Probabilistic Mechanics, and Structural and Geotechnical Reliability*, Denver, CO, July 8-10, 1992.
Richter, C. F. (1958). *Elementary Seismology*, W. H. Freeman, San Francisco, CA.
Rosenblueth, E. (1957). Comments on torsion, in *Proc. of the Convention of the Structural Engineers Association of Southern California*, 36-38.
Trifunac, M. D. (1982). A note on rotational components of earthquake motions on ground surface for incident body waves, *Soil Dyn. Earthquake Engng.* 1, 11-19.
Trifunac, M. D., and V. W. Lee (1997). Peak surface strains during strong earthquake motion, *Soil Dyn. Earthquake Engng.* 15, 311-319.
Zeng, Y., K. Aki, and T.-L. Teng (1993). Mapping of the high-frequency source radiation for the Loma Prieta earthquake, California, *J. Geophys. Res.* 98, 11981-11993.